

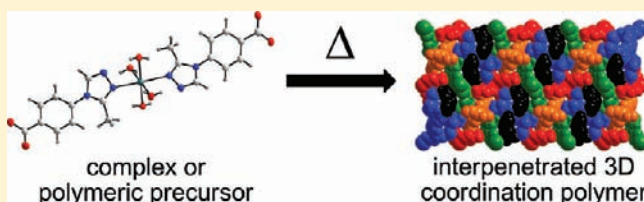
Solid-State Syntheses of Coordination Polymers by Thermal Conversion of Molecular Building Blocks and Polymeric Precursors

Daniel Lässig, Jörg Lincke, Renata Gerhardt, and Harald Krautscheid*

Universität Leipzig, Fakultät für Chemie und Mineralogie, Johannisallee 29, D-04103 Leipzig, Germany

Supporting Information

ABSTRACT: The syntheses and crystal structures of a mononuclear cadmium complex and five novel coordination polymers based on 1,2,4-triazolyl benzoates are presented. The compounds ${}^3[\text{Cd}(\text{H-Me-trz-pba})_2]$ (2), ${}^3[\text{Cd}(\text{Me-3py-trz-pba})_2]$ (4), and ${}^3[\text{Zn}(\text{H-Me-trz-pba})_2]$ (6) can be obtained by solvothermal synthesis or simple heating of the starting materials in appropriate solvents, and are also accessible by thermal conversion of the complex $[\text{Cd}(\text{H-Me-trz-pba})_2(\text{H}_2\text{O})_4]$ (1), the one-dimensional (1D) coordination polymer ${}^1[\text{Cd}(\text{Me-3py-trz-pba})_2(\text{H}_2\text{O})_2] \cdot \text{H}_2\text{O}$ (3), and the porous three-dimensional (3D) framework ${}^3[\text{Zn}(\text{H-Me-trz-pba})_2] \cdot 4\text{H}_2\text{O}$ (5), respectively. The driving force for these conversions is the formation of thermally stable, nonporous, crystalline 3D coordination polymers. The structural transformations are accompanied by the loss of water and reveal significant changes of the coordination spheres of the metal ions caused by a rearrangement of the triazolyl benzoate ligands. Compounds 2, 4, 5, and 6 exhibit 4- and 5-fold interpenetration of diamondoid networks (*dia*) and are thermally stable up to 380 °C.



INTRODUCTION

Metal–organic frameworks (MOFs) have gained increasing interest, because of their high diversity of possible structures. Because of their distinct properties as porous materials, this novel class of hybrid materials exhibits a high potential for such applications as gas separation and storage,^{1–6} sensors,^{7,8} and heterogeneous catalysis.⁹

Topological analyses are commonly used to classify this wide field of possible framework structures.^{10–12} Despite the fact that coordination polymers often form complex structures, a large percentage of published networks can be simplified to the topologies of basic inorganic compounds.^{10,12,13} The most common, especially for interpenetrated frameworks (29.9%), is the diamondoid topology (*dia*) with the point symbol $\{6^6\}$.¹⁴ In many cases of porous diamondoid networks, interpenetration leads to a significant reduction of porosity, but is also accompanied by an enhanced thermal stability, because of additional stabilizing interactions (hydrogen bonding, $\pi \cdots \pi$ interactions) between the interwoven nets.^{12,13}

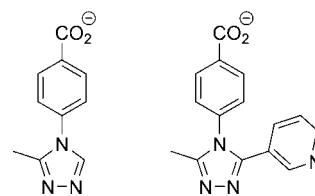
For numerous molecular compounds, the phenomenon of polymorphism is observed. In these cases, different crystal structures can be found, because of varying packing interactions between the respective molecules.¹⁵ An extended interpretation of this concept introduces the term of supramolecular isomerism, which is used for networks with the same composition but with different topologies.^{15,16}

The potential of MOFs forming highly ordered porous structures has been impressively shown by the isorecticular series of Yaghi and co-workers,¹⁷ the well-known HKUST-1 ($\text{Cu}_3(\text{btc})_2$, where *btc* = 1,3,5-benzene tricarboxylate)^{2,18} and the MIL series of Férey et al.^{19–21} Apart from pure carboxylates, ligands with a combination of nitrogen-containing heterocycles such as 1,2,4-

triazoles and pyridines were found to exhibit promising coordination chemistry for the synthesis of MOFs.^{5,22,23}

Based on two substituted 1,2,4-triazolyl benzoates²⁴ (Chart 1), we herein present the syntheses and crystal structures of a

Chart 1. The Ligands $(\text{H-Me-trz-pba})^-$ and $(\text{Me-3py-trz-pba})^-$



cadmium complex as well as five zinc and cadmium coordination polymers. Furthermore, we report on the conversion of complexes, coordination polymers of lower dimensionality and porous networks into crystalline, interpenetrated 3D coordination polymers with a high thermal stability up to 380 °C. To our best knowledge, a systematic investigation of such thermal conversions of suitable precursors to 3D coordination polymers based on full rearrangements of the coordination spheres of the metal ions and the loss of solvent molecules has not been reported so far.

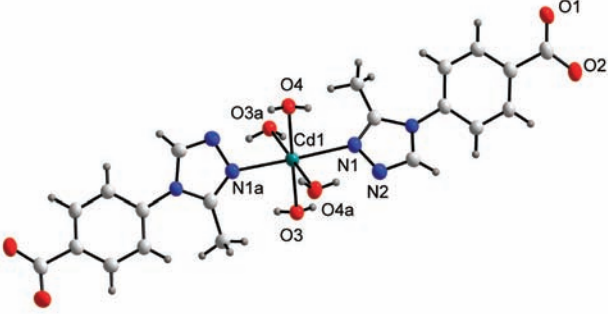
RESULTS AND DISCUSSION

From $[\text{Cd}(\text{H-Me-trz-pba})_2(\text{H}_2\text{O})_4]$ (1) to ${}^3[\text{Cd}(\text{H-Me-trz-pba})_2]$ (2). The complex $[\text{Cd}(\text{H-Me-trz-pba})_2(\text{H}_2\text{O})_4]$ (1) was

Received: February 1, 2012

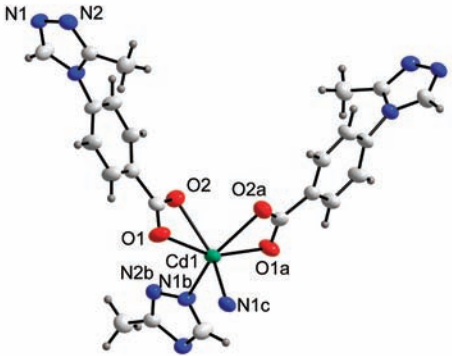
Published: May 16, 2012

Table 1. Selected Bond Lengths and Angles of **1**^a

		1	
		bond length [pm]	
	Cd1-O3	231.9(3)	
	Cd1-O4	236.7(2)	
	Cd1-N1	230.7(2)	
		angle [°]	
	O3-Cd1-O3a	85.7(1)	
	O3-Cd1-O4	178.90(6)	
	O3-Cd1-N1	91.14(8)	
	N1-Cd1-N1a	170.1(1)	

^aSymmetry codes for **1**: $a: 0.5 - x, y, 1 - z$.

Table 2. Selected Bond Lengths and Angles of **2**^a

		2	
		bond length [pm]	
	Cd1-O1	235.0(4)	
	Cd1-O2	239.6(7)	
	Cd1-N1b	227.7(5)	
		angle [°]	
	O1-Cd1-O1a	154.6(2)	
	O1-Cd1-O2	56.0(1)	
	O1-Cd1-O2a	103.3(2)	
	O1-Cd1-N1b	105.4(2)	
	O1-Cd1-N1c	92.1(2)	
	O2-Cd1-N1c	147.5(2)	
	N1b-Cd1-N1c	92.8(3)	

^aSymmetry codes for **2**: $a: 1 - x, 1 - y, z; b: 1.25 - x, -0.25 + y, -1.25 + z; c: -0.25 + x, 1.25 - y, -1.25 + z$.

obtained from $\text{Cd}(\text{OAc})_2 \cdot 2\text{H}_2\text{O}$ and $\text{H}(\text{H-Me-trz-pba})$ in $\text{H}_2\text{O}/\text{MeCN}$ (1:1, v/v) by diffusion at room temperature after 21 days. Compound **1** crystallizes in the monoclinic space group $I2/a$ (No. 15) with four formula units per unit cell. (Bond lengths and bond angles for **1** are given in Table 1.) The Cd^{2+} ion is distorted octahedrally coordinated by two monodentate triazole units of $(\text{H-Me-trz-pba})^-$ in *trans* orientation and four water molecules.

Whereas **1** is only accessible via diffusion, single crystals of $^3_\infty[\text{Cd}(\text{H-Me-trz-pba})_2]$ (**2**) were obtained from $\text{Cd}(\text{OAc})_2 \cdot 2\text{H}_2\text{O}$ and the protonated ligand under solvothermal conditions. (Bond lengths and bond angles for **2** are given in

Table 2.) In addition, phase-pure microcrystalline material of **2** can be synthesized in multigram scale by reflux of $\text{Cd}(\text{OAc})_2 \cdot 2\text{H}_2\text{O}$ and $\text{H}(\text{H-Me-trz-pba})$ in $\text{H}_2\text{O}/\text{MeCN}$ (1:1, v/v) for 48 h (see Figure SI-13 in the Supporting Information). **2** crystallizes in the noncentrosymmetric orthorhombic space group $Fdd2$ (No. 43) with eight formula units per unit cell. The Cd^{2+} ion resides on the 2-fold axis and is highly distorted octahedrally coordinated by two monodentate 1,2,4-triazole units and by two chelating carboxylate groups.

For the neutral network of **2**, the common **dia** topology (point symbol $\{6^6\}$) is built up by the linkage of the Cd^{2+} ions

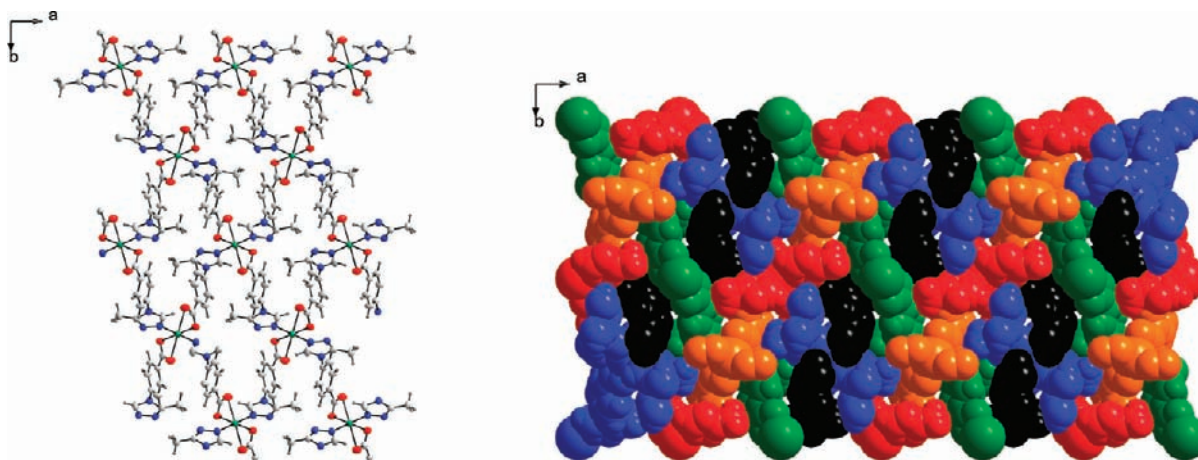


Figure 1. Single-net (50% ellipsoids, left) and space-filling projection of five interpenetrated nets of **2** (right).

Scheme 1. Reaction Conditions for the Syntheses of **1** and **2**

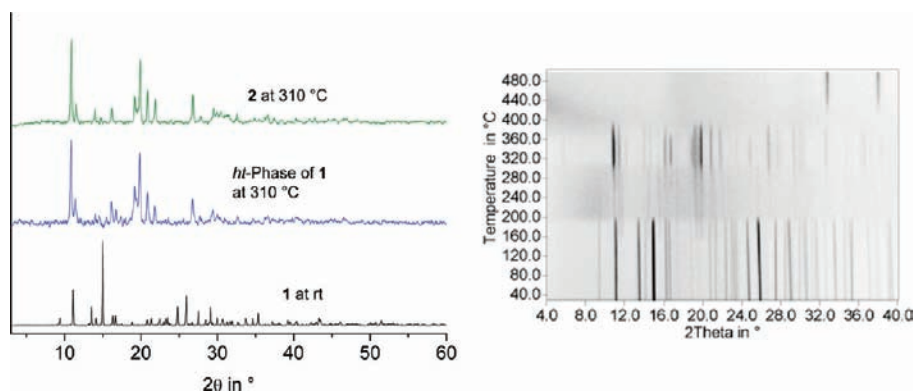
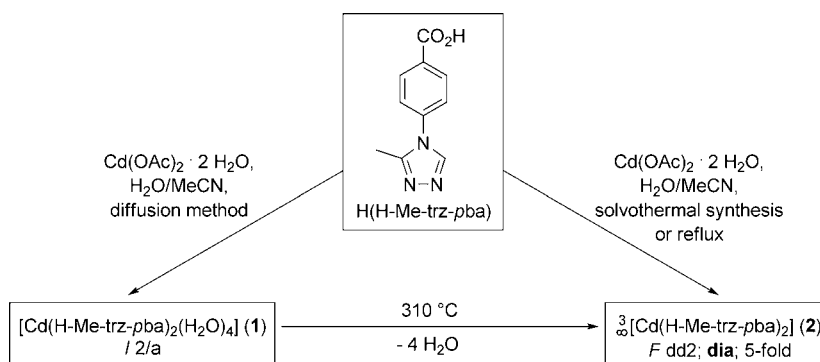


Figure 2. (Left) Comparison of the powder X-ray patterns of **1** and **2** (Cu Kα₁; λ = 154.060 pm). (Right) Temperature-dependent powder diffraction pattern (Guinier–Simon diagram) of **1**.

as four-connected nodal points. In addition, a 5-fold interpenetration of type Ia with a full interpenetration vector (FIV) of 709 pm in the crystallographic *c*-direction was found, leading to a non-porous network with no solvent accessible voids.^{13,15,25,26} (Graphic depictions of **2** are shown in Figure 1.)

Beside the described synthesis routes, phase-pure **2** can be obtained via the thermal conversion of **1** under the loss of solvent molecules (Scheme 1).

As can be seen from the temperature-dependent powder X-ray diffraction pattern (TD-PXRD), **1** is thermally stable up to 200 °C. In the temperature region of 200–310 °C, an amorphous phase is observed. Above 310 °C, a crystalline phase with a new powder pattern is detected, which can be

assigned to compound **2** (see Figure 2). The newly formed 5-fold interpenetrated coordination polymer **2** eventually remains intact up to a temperature of 380 °C.

This conversion is confirmed by DTA/TG-MS analysis (see Figure 3). Up to 170 °C a mass loss of 12.2% was found, which correlates perfectly with the calculated weight loss of 12.2% for four water molecules per formula unit, indicated by the MS signal *m/z* = 18. In compliance with TD-PXRD, thermogravimetry reveals a thermal stability of **2** up to 380 °C. Above this temperature, **2** decomposes under the release of carbon dioxide (*m/z* = 44). Therefore, it can be concluded that, after the loss of the four water molecules per formula unit of **1**, a full rearrangement of ligands and metal ions occurred, leading to the

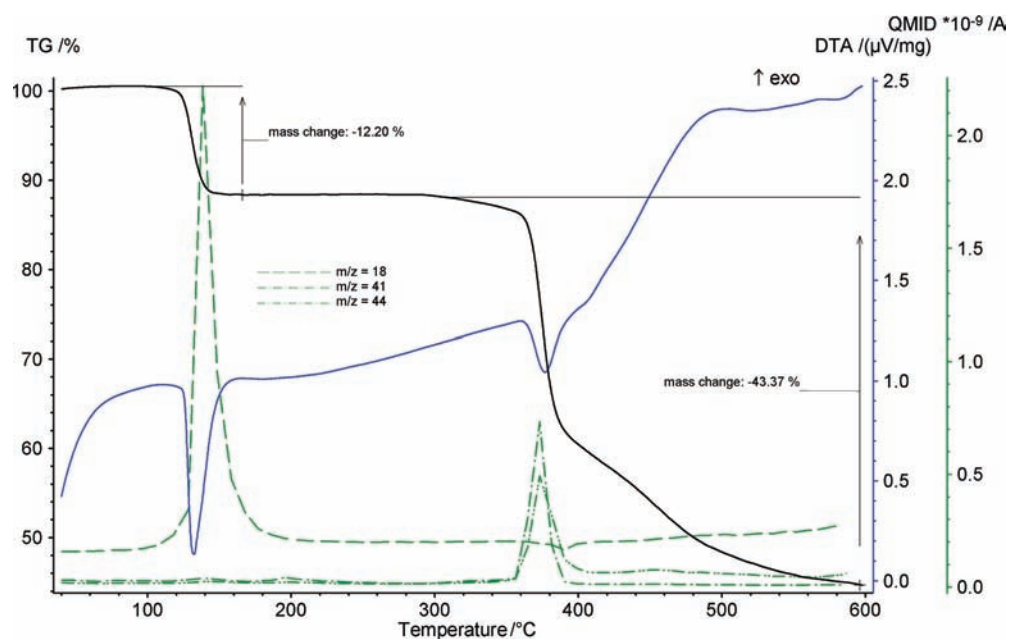


Figure 3. DTA/TG-MS analysis of **1**. The black trace represents the thermogravimetry (TG) signal, while the blue trace represents the differential thermal analysis (DTA) signal and the green traces represent the mass spectroscopy (MS) signals.

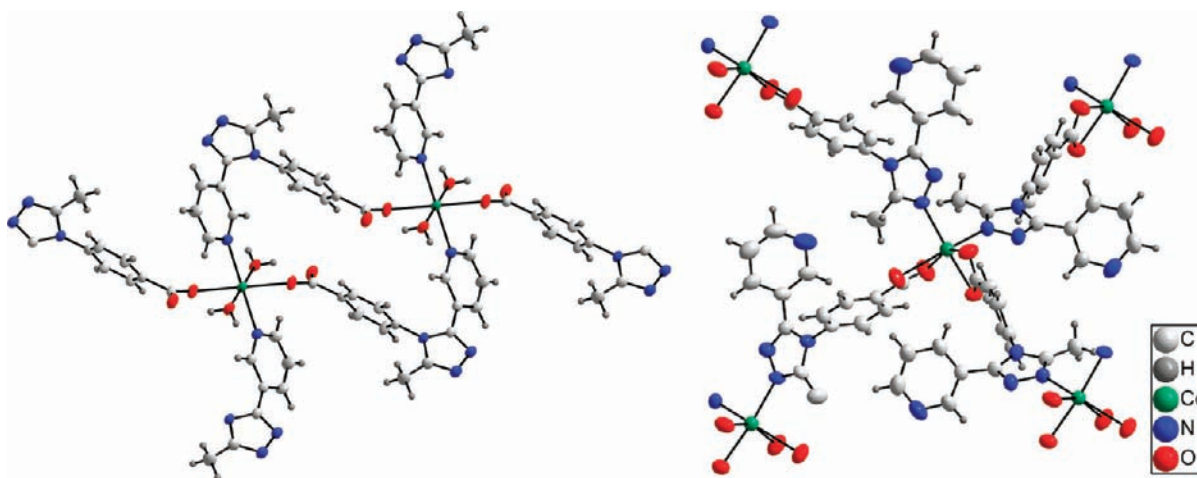


Figure 4. Part of the crystal structures of **3** (left) and **4** (right).

formation of the three-dimensional network of **2**. Within this rearrangement, all coordinative bonds are broken and reformed, which is evidenced by the change of the coordination mode. Whereas in **1**, the ligand coordinates with the electronically favored nitrogen atom (+I-effect of the methyl group), in **2**, coordination of the sterically less-shielded nitrogen atom is observed.

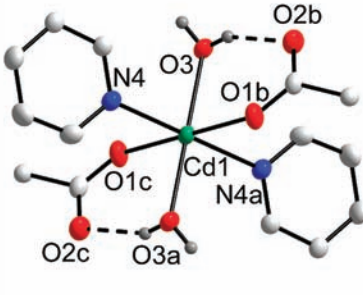
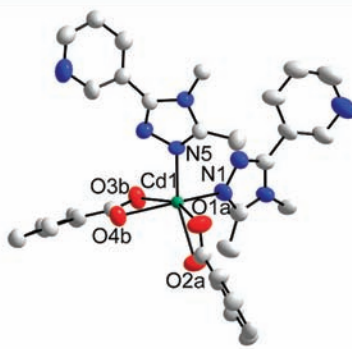
From ${}^1[\text{Cd}(\text{Me-3py-trz-pba})_2(\text{H}_2\text{O})_2]\cdot\text{H}_2\text{O}$ (**3**) to ${}^3[\text{Cd}(\text{Me-3py-trz-pba})_2]$ (**4**). In the case of the ligand (Me-3py-trz-pba)[−], a similar relation between the products ${}^1[\text{Cd}(\text{Me-3py-trz-pba})_2(\text{H}_2\text{O})_2]\cdot\text{H}_2\text{O}$ (**3**) and ${}^3[\text{Cd}(\text{Me-3py-trz-pba})_2]$ (**4**) can be found. The reactions of equimolar amounts of the protonated ligand and Cd(OAc)₂·2H₂O in H₂O/MeCN (1:1, v/v) under solvothermal conditions or by simple reflux lead to phase-pure compound **3** (see Figure SI-14 in the Supporting Information). If the solvent mixture is replaced by dimethylformamide (DMF), the three-dimensional (3D) coordination polymer **4** is obtained.

Whereas **3** crystallizes in the triclinic space group $P\bar{1}$ (No. 2) with one formula unit per unit cell, **4** crystallizes in the

monoclinic acentric space group Pc (No. 7) with two formula units per unit cell. In **3**, the Cd²⁺ ion is located on the inversion center and is distorted octahedrally coordinated by two monodentate carboxylates, two water molecules, and two pyridine rings in *trans* orientation (Figure 4). In addition, strong intramolecular hydrogen bonds with an O⋯O distance of 260.9(4) pm (see Table 3) between the noncoordinating oxygen atoms of the carboxylates and the aquo ligands are observed. Hence, the positions of the carboxylate groups are fixed.

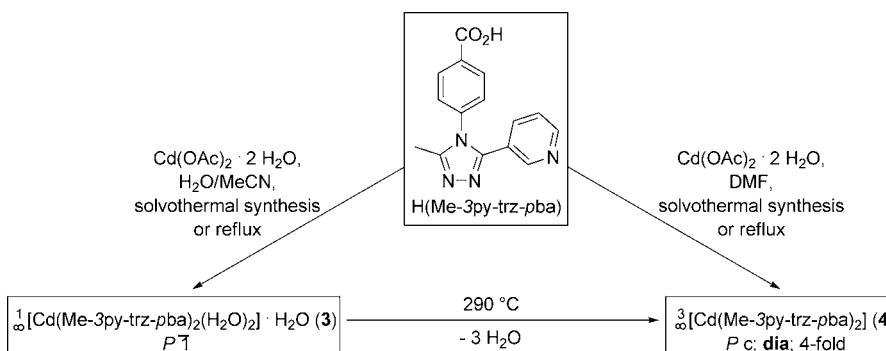
In contrast to the one-dimensional (1D) coordination polymer **3**, **4** represents a three-dimensional coordination polymer with 4-fold interpenetration. The Cd²⁺ ion is distorted octahedrally coordinated by two monodentate triazole units in *cis*-orientation and chelating carboxylate groups, the pyridine rings do not interact with the metal ions. Therefore, the ligands act as linear linkers leading to a network with the point symbol {6⁶} and *dia* topology. Whereas a single framework possesses a high porosity, the four interwoven nets lead to an almost

Table 3. Selected Bond Lengths and Angles of 3 and 4^a

3		4	
			
	bond length [pm]		bond length [pm]
Cd1-O1b	229.0(2)	Cd1-N1	229.7(7)
Cd1-O3	230.0(2)	Cd1-N5	228.5(7)
Cd1-N4	237.5(3)	Cd1-O1a	231.9(7)
O2b...O3	260.9(4)	Cd1-O2a	243.7(6)
		Cd1-O3b	234.1(6)
		Cd1-O4b	234.8(6)
	angle [°]		angle [°]
O1b-Cd1-O3	88.01(9)	N1-Cd1-N5	96.8(3)
O1b-Cd1-N4	95.23(9)	N1-Cd1-O1a	108.4(3)
O3-Cd1-N4	92.4(1)	N1-Cd1-O3b	91.4(3)
		N5-Cd1-O3b	103.9(3)
		O1a-Cd1-O3b	155.2(3)
		O1a-Cd1-O4b	100.7(3)

^aSymmetry codes for 3: *a*: 1 - *x*, -*y*, -*z*; *b*: 1 - *x*, 1 - *y*, -*z*; *c*: *x*, -1 + *y*, *z*. Symmetry codes for 4: *a*: -1 + *x*, 1 - *y*, -0.5 + *z*; *b*: 1 + *x*, 2 - *y*, -0.5 + *z*.

Scheme 2. Reaction Conditions for the Syntheses of 3 and 4



nonporous coordination polymer with only 5% solvent accessible voids.²⁶ Cobalt and zinc frameworks isomorphous to 4 were presented recently.²⁷

Similar to the conversion of 1 into 2, 4 can be obtained by loss of 3 equivalents of water upon heating of the 1D coordination polymer 3. (See Scheme 2.) As can be seen from TD-PXRD measurements, 3 is stable up to 230 °C. Above this temperature, again, an amorphous phase is observed. When the sample is heated up to 290 °C, discrete reflections occur,

indicating a crystalline phase with stability of the framework up to 380 °C. The powder patterns of 4 and the crystalline high-temperature phase of 3 are in perfect agreement. (See Figure 5.) Therefore, it can be concluded that the 1D polymer 3 is converted to the 3D diamondoid network of 4 within the temperature range of 230–290 °C. Again, this conversion is accompanied by a rearrangement in the Cd²⁺ coordination sphere. Whereas in 3, the pyridine groups of the (Me-3py-trz-pba)⁻ ligands coordinate, in 4 the triazole units bind to the metal ions.

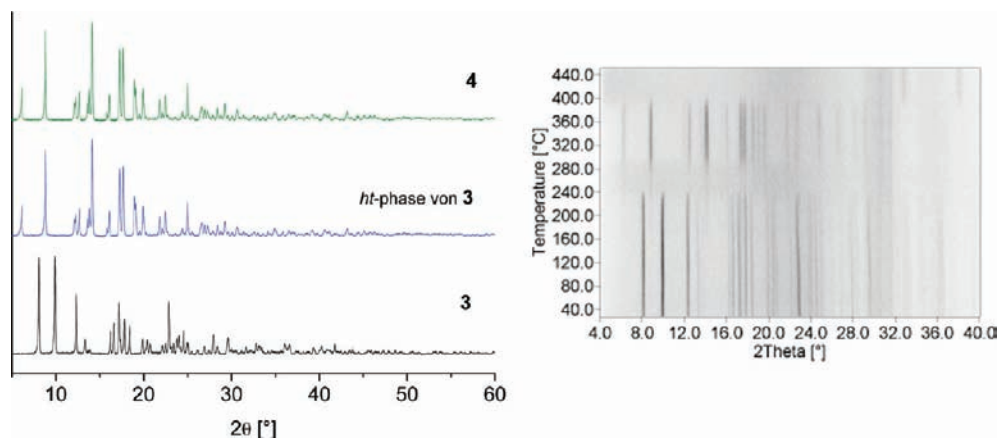


Figure 5. (Left) Comparison of the powder patterns of 3, 4, and the high-temperature phase of 3 (room-temperature measurements). (Right) Temperature-dependent powder patterns (Guinier–Simon diagram) of 3.

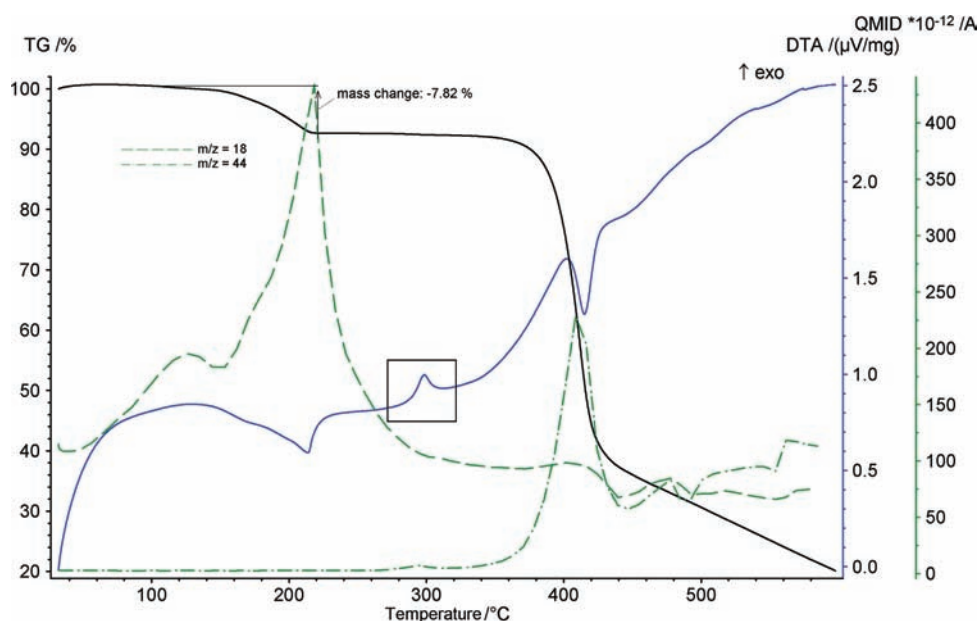


Figure 6. DTA/TG-MS analysis of 3. Black trace represents the TG signal, while the blue trace represents the DTA signal and the green trace represents the MS signals.

The conversion is evidenced by the loss of water molecules retraced by DTA/TG-MS analysis. Up to 230 °C, a mass loss of 7.8% is observed, which correlates well with the calculated mass loss of 7.5% for three water molecules per formula unit ($m/z = 18$). The phase transition from crystalline 3 to the amorphous phase and the decomposition of 4 at ~ 390 °C ($m/z = 44$ [CO_2] $^+$) are found to be endothermic. The exothermic peak at 290–300 °C in the DTA curve (black square, Figure 6) can be interpreted as the crystallization of 4 from the amorphous material.

Conversions within the System of ${}^3[\text{Zn}(\text{H-Me-trz-pba})_2]$. Also within the system of three diamondoid networks (**dia**) of ${}^3[\text{Zn}(\text{H-Me-trz-pba})_2]$ (**5**, **6**, and **6-ht**), thermal treatment leads to conversions. Compound ${}^3[\text{Zn}(\text{H-Me-trz-pba})_2] \cdot 4\text{H}_2\text{O}$ (**5**) crystallizes in the tetragonal space group $P4nc$ (No. 104) with four formula units per unit cell. The asymmetric unit contains a $(\text{H-Me-trz-pba})^-$ ligand and a Zn^{2+} ion residing on a 2-fold axis. Furthermore, approximately two disordered and partially occupied water molecules could be located during the refinement process. Nevertheless, from TG-DTA-MS

measurements, the water content was determined to be four water molecules per formula unit (see Figure SI-18 in the Supporting Information). In the crystal structure of **5**, the Zn^{2+} ion is coordinated in a distorted tetrahedral fashion by two monodentate carboxylate groups and two triazole rings (see Table 4). Phase-pure **5** can only be obtained by reacting equimolar amounts of $\text{Zn}(\text{OAc})_2 \cdot 2\text{H}_2\text{O}$ and $\text{H}(\text{H-Me-trz-pba})$ in $\text{H}_2\text{O}/\text{MeOH}$ (1:1, v/v) by diffusion at room temperature (see Scheme 3). Whereas **2** and **4** show an interpenetration of type Ia (FIV), **5** can be assigned to be of type IIIa, since the interwoven nets are not only connected by simple translation. In addition to the translation interpenetration vector (TIV) in $[001]$ with a length of 1288 pm, the c glide plane (NISE) acts as a second independent symmetry element between two pairs of networks. Despite the 4-fold interpenetration, **5** possesses pore channels along the crystallographic c -direction with squarish windows of 400 pm \times 400 pm and a solvent-accessible volume of $\sim 34\%$.²⁶ (See Figure 7.)

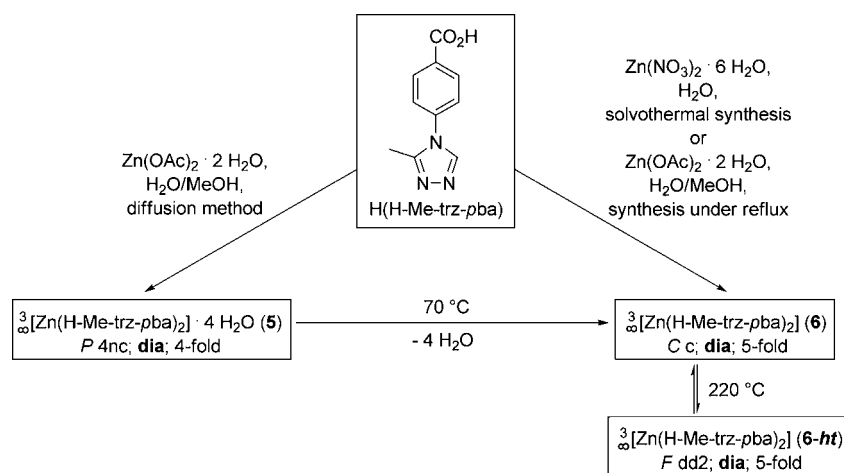
As can be seen from TD-PXRD measurements (Figure 8), **5** undergoes a phase transition already at 70 °C. The high-temperature

Table 4. Selected Bond Lengths and Angles of 5 and 6^a

5		6	
	bond length [pm]		bond length [pm]
Zn1-O1	196.6(4)	Zn1-O1	196.7(2)
Zn1-N1b	200.9(4)	Zn1-O3	198.6(2)
		Zn1-N1a	208.1(3)
		Zn1-N4b	202.9(3)
	angle [°]		angle [°]
O1-Zn1-O1a	100.8(2)	O1-Zn1-O3	107.5(1)
O1-Zn1-N1b	109.5(2)	O1-Zn1-N1a	105.6(1)
O1-Zn1-N1c	105.8(2)	O1-Zn1-N4b	124.0(1)
		O3-Zn1-N1a	98.6(1)
		O3-Zn1-N4b	117.4(1)
		N1a-Zn1-N4b	99.3(1)

^aSymmetry codes for 5: a: 1 - x, 2 - y, z; b: 1.5 - x, 0.5 + y, -0.5 + z; c: -0.5 + x, 1.5 - y, -0.5 + z. Symmetry codes for 6: a: -1 + x, 1 - y, 0.5 + z; b: -1.5 + x, 0.5 - y, -0.5 + z.

Scheme 3. Reaction Conditions for the Syntheses of 5 and 6



phase can be assigned to compound 6 (Figure 8), a new diamondoid network of $\text{3}_{\infty}[\text{Zn}(\text{H-Me-trz-pba})_2]$ without any

porosity.²⁶ In contrast to the conversions between 1 and 2 or 3 and 4, no amorphous phase between 5 and 6 is observed.

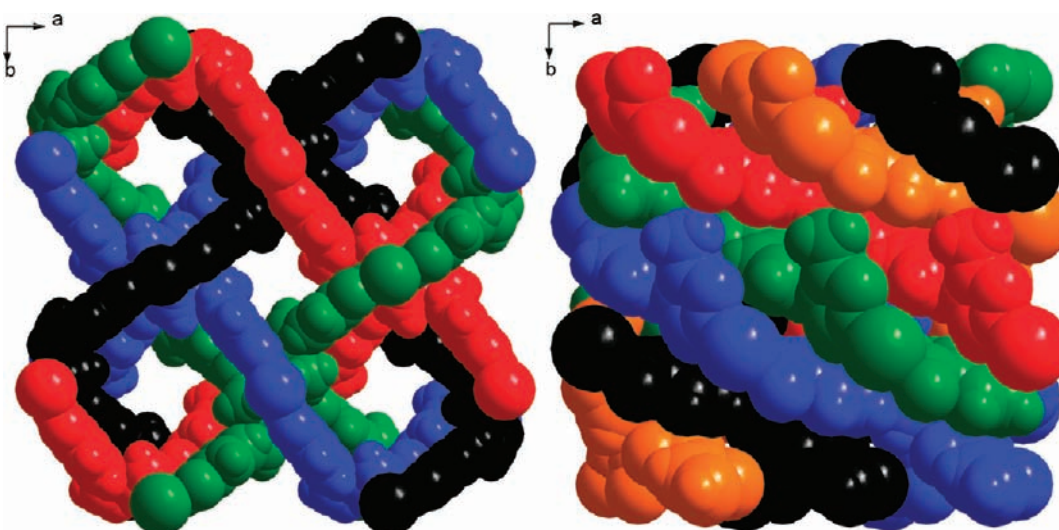


Figure 7. Space-filling models of **5** and **6** (views are along the crystallographic *c*-direction).

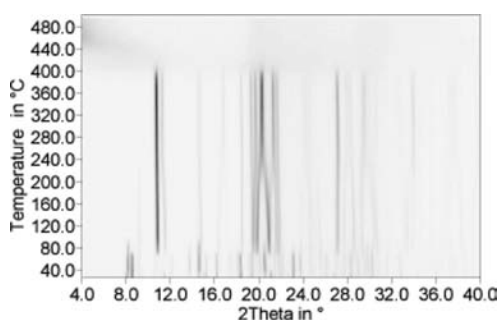


Figure 8. Temperature-dependent powder X-ray diffraction (TD-PXRD) pattern (Guinier–Simon diagram) of ${}^3_{\infty}[\text{Zn}(\text{H-Me-trz-pba})_2] \cdot 4\text{H}_2\text{O}$ (**5**).

Polymer **6** can directly be synthesized from $\text{Zn}(\text{NO}_3)_2 \cdot 6\text{H}_2\text{O}$ and $\text{H}(\text{H-Me-trz-pba})$ under hydrothermal conditions (Scheme 3). In addition, microcrystalline material is accessible in multigram scale by simple reflux of $\text{Zn}(\text{OAc})_2 \cdot 2\text{H}_2\text{O}$ and the protonated ligand in $\text{H}_2\text{O}/\text{MeOH}$ (1:1, v/v) (see Figure SI-15 in the Supporting Information).

Polymer **6** crystallizes in the monoclinic space group *Cc* (No. 9) with four formula units per unit cell. Similar to **5**, the Zn^{2+} ions are distorted tetrahedrally coordinated by two monodentate triazole units and two carboxylates (see Table 4), forming a 3D network with *dia* topology.

The conversion of compound **5** into **6** occurs in a system of interpenetrated networks, accompanied by a change in degree of interpenetration already at 70 °C. In contrast to the framework of **5** with four interwoven nets, a 5-fold interpenetration of type Ia is found for **6**. This leads to the conclusion that coordinative bonds between the ligands and the Zn ions must be broken in order to enable the observed phase transition. This is confirmed by the coordination mode of the triazole unit: in **5**, the triazole coordinates with the sterically more hindered, but electronically favored nitrogen atom; in **6**, the sterically favored nitrogen atom binds to the Zn^{2+} ion. In comparison to **6**, **5** shows significantly shorter $\text{Zn}-\text{N}_{\text{trz}}$ bond lengths originating in the methyl group located in α -position to the coordinating nitrogen atom. The driving force for this conversion is mainly the loss of water molecules and the formation of a crystalline network without any porosity.

To the best of our knowledge, crystal-to-crystal transformations combined with a change of the number of interpenetrating nets are a very rare phenomenon. An example is $[\text{Ag}_6\text{Cl}(\text{atz})_4] \cdot \text{OH} \cdot 6\text{H}_2\text{O}$ (*atz* = 3-amino-1,2,4-triazolate), which shows a change in interpenetration between 5-fold and 6-fold.²⁸

Further thermal treatment of **5** leads to a second phase transition at 220 °C (Figure 8), during which certain reflections become identical. Indexing of the powder pattern of this high-temperature (*ht*) phase of **6** identifies it to be the isomorphous zinc analogue ${}^3_{\infty}[\text{Zn}(\text{H-Me-trz-pba})_2]$ (**6-ht**) of the cadmium coordination polymer **2**. In contrast to the sharp phase transition at 70 °C, the reversible conversion of **6** to **6-ht** occurs more gradually over a temperature range. As expected for this phase transition, the space group *Cc* of the low-temperature phase **6** is a subgroup of *Fdd2* (**6-ht**). Based on the reversibility, and from comparison with **2**, it can be concluded that, for the transition from **6** to **6-ht**, the connectivity in the network is retained. The **6-ht** compound is thermally stable up to 420 °C. Whereas the conversions of **1** to **2**, **3** to **4**, and **5** to **6** are initiated by the entropically favored loss of water molecules, the crystallization of **2** and **4** from amorphous phases and the transformation from **6** to **6-ht** can be regarded as enthalpy-driven.

CONCLUSION

The mononuclear complex $[\text{Cd}(\text{H-Me-trz-pba})_2(\text{H}_2\text{O})_4]$ (**1**), the one-dimensional (1D) coordination polymer ${}^1_{\infty}[\text{Cd}(\text{Me-3py-trz-pba})_2(\text{H}_2\text{O})_2] \cdot \text{H}_2\text{O}$ (**3**) and four zinc- and cadmium-containing diamondoid frameworks (**2**, **4**, **5**, and **6**) have been synthesized from the protonated ligands and the respective metal salts. A topological analysis reveals $\{6^6\}$ diamondoid (*dia*) topology in the case of all these networks, but varying 4-fold (**4** and **5**) and 5-fold (**2** and **6**) interpenetration. Such highly interpenetrated networks are rarely observed (from recent TOPOS statistics: 4-fold, 8.3%; 5-fold, 3.6%), in comparison with the regularly occurring 2-fold (60.6%) and 3-fold interpenetration (21.5%). (Table 5 shows the crystallographic data for compounds **1–6**.)

Their thermal behavior shows that suitable complexes or 1D coordination polymers with aquo ligands such as **1** or **3** can be converted to neutral, three-dimensional (3D), interpenetrated coordination polymers during the loss of solvent molecules.

Table 5. Crystallographic Data for [Cd(H-Me-trz-pba)₂(H₂O)₄] (1), ³_∞[Cd(H-Me-trz-pba)₂] (2), ¹_∞[Cd(Me-3py-trz-pba)₂(H₂O)₂]·H₂O (3), ³_∞[Cd(Me-3py-trz-pba)₂] (4), ³_∞[Zn(H-Me-trz-pba)₂]·4H₂O (5), and ³_∞[Zn(H-Me-trz-pba)₂] (6)²⁹

compound	1	2	3	4	5	6
color	colorless	colorless	colorless	colorless	colorless	colorless
shape	prism	needle	needle	prism	prism	needle
crystal dimensions [mm]	0.08 × 0.20 × 0.50	0.11 × 0.13 × 0.50	0.11 × 0.13 × 0.31	0.18 × 0.21 × 0.22	0.50 × 0.50 × 0.50	0.14 × 0.16 × 0.50
formula	CdC ₂₀ H ₂₄ N ₆ O ₈	CdC ₂₀ H ₁₆ N ₆ O ₄	CdC ₃₀ H ₂₈ N ₈ O ₇	Cd C ₃₀ H ₂₂ N ₈ O ₄	ZnC ₂₀ H _{20.25} N ₆ O _{6.125}	ZnC ₂₀ H ₁₆ N ₆ O ₄
MW [g mol ⁻¹]	588.85	516.79	725.00	670.92	508.04	469.76
temperature [K]	180(2)	180(2)	213(2)	180(2)	213(2)	213(2)
diffractometer	STOE IPDS-2T	STOE IPDS-2T	STOE IPDS-I	STOE IPDS-2T	STOE IPDS-I	STOE IPDS-I
crystal system	monoclinic	orthorhombic	triclinic	monoclinic	tetragonal	monoclinic
space group	<i>I</i> 2/ <i>a</i> (No. 15)	<i>Fdd</i> 2 (No. 43)	<i>P</i> $\bar{1}$ (No. 2)	<i>Pc</i> (No. 7)	<i>P4nc</i> (No. 104)	<i>Cc</i> (No. 9)
unit cell						
<i>a</i> [pm]	1896.9(2)	1899.5(2)	779.2(1)	740.0(1)	1459.6(2)	664.74(9)
<i>b</i> [pm]	717.96(5)	3006.3(3)	935.7(2)	1461.5(3)		1916.7(2)
<i>c</i> [pm]	1598.8(2)	709.04(6)	1169.5(2)	1417.5(3)	1288.4(1)	1536.6(3)
α [°]			77.41(1)			
β [°]	93.636(9)		71.00(1)	99.54(1)		98.54(1)
γ [°]			73.42(1)			
volume [$\times 10^6$ pm ³]	2173.0(4)	4048.9(7)	765.3(2)	1511.8(5)	2744.7(5)	1936.0(5)
<i>Z</i>	4	8	1	2	4	4
density [g cm ⁻³]	1.800	1.696	1.573	1.474	1.229	1.612
μ (Mo <i>K</i> α) [mm ⁻¹]	1.068	1.120	0.774	0.771	0.936	1.311
θ_{\min} – θ_{\max} [°]	1.04–28.00	1.15–28.00	1.65–25.00	0.96–26.00	1.90–28.00	1.90–27.00
reflections measured	9747	3597	5489	7462	7131	4644
independent reflections	2620	1992	2546	4596	3019	3291
observed reflections (<i>I</i> > 2 σ (<i>I</i>))	2476	1827	2352	3383	1901	3141
<i>R</i> _{int}	0.0353	0.0525	0.0292	0.0451	0.0368	0.0448
parameters refined	173	143	221	391	163	182
<i>R</i> ₁ (<i>I</i> > 2 σ (<i>I</i>))	0.0432	0.0478	0.0309	0.0467	0.0541	0.0280
<i>wR</i> ₂ (all data)	0.1178	0.1289	0.0818	0.1349	0.1582	0.0718
Flack- <i>x</i> parameter		0.02(1)		–0.05(4)	0.03(5)	–0.01(1)
max/min peak [$\times 10^{-6}$ pm ⁻³]	1.1/–0.8	0.9/–1.5	1.3/–0.3	0.8/–0.7	0.8/–0.4	0.4/–0.4

Both products **2** and **4** represent interpenetrated, nonporous frameworks with **dia** topology.

As shown by compounds **5** and **6**, conversions based on thermal treatment can even take place within a system of interpenetrated frameworks. The driving force for the presented conversions is mainly the formation of thermally stable, nonporous, crystalline 3D coordination polymers. In the case of **2** and **4**, a remarkable thermal stability up to 380 °C is reached. In addition, the conversion of the hydrates **1**, **3**, and **5** is entropically favored by the loss of water molecules.

The observed transformations are accompanied by a change in the coordination spheres of the metal ions. Remarkably, different pathways for these solid-state reactions are detected. Whereas the conversion from **5** to **6** occurs directly at 70 °C, for the transitions of **1** to **2** and **3** to **4**, an intermediate amorphous phase is observed. After rearrangement of all components in temperature ranges of 200–310 °C (**1**) and 230–290 °C (**3**), highly crystalline 3D materials are found. Furthermore, the structural transformation from **6** to **6-ht** was found to be reversible.

As can be seen from the reaction schemes, the structures of coordination polymers can be very sensitive, with respect to the synthesis conditions applied. Compounds **1** and **5** verify that milder reaction conditions, especially diffusion methods at room temperature, allow the synthesis of thermodynamically less-stable products than solvothermal reactions or synthesis under reflux.

■ ASSOCIATED CONTENT

📄 Supporting Information

Experimental details associated with this article can be found in the online version. Cambridge Crystallographic Data Centre (CCDC) File Nos. 751491 and 861641–861649 contain the supplementary crystallographic data for this paper. These data can be obtained free of charge from the Cambridge Crystallographic Data Centre via www.ccdc.cam.ac.uk/data_request/cif. This material is available free of charge via the Internet at <http://pubs.acs.org>.

■ AUTHOR INFORMATION

✉ Corresponding Author

*E-mail: Krautscheid@rz.uni-leipzig.de

Notes

The authors declare no competing financial interest.

■ ACKNOWLEDGMENTS

We thank M.Sc. Marcel Handke for the DTA/TG-MS analyses. Financial support by Deutsche Forschungsgemeinschaft (DFG SPP 1362 - Poröse metallorganische Gerüstverbindungen), the University of Leipzig (PbF-1) and the graduate school BuildMoNa is gratefully acknowledged. D.L. acknowledges the fellowship of the Fonds der Chemischen Industrie, and J.L. acknowledges the ESF fellowship. Funded by the European Union and the Free State of Saxony.

■ DEDICATION

Dedicated to Prof. Dr. Reinhard Kirmse on the occasion of his 65th birthday.

■ REFERENCES

- (1) D'Alessandro, D. M.; Smit, B.; Long, J. R. *Angew. Chem., Int. Ed.* **2010**, *49*, 2–27.
- (2) Hartmann, M.; Kunz, S.; Himsl, D.; Tangermann, O.; Ernst, S.; Wagener, A. *Langmuir* **2008**, *24*, 8634–8642.
- (3) Debatin, F.; Thomas, A.; Kelling, A.; Hedin, N.; Bacsik, Z.; Senkovska, I.; Kaskel, S.; Junginger, M.; Müller, H.; Schilde, U.; Jäger, C.; Friedrich, A.; Holdt, H.-J. *Angew. Chem., Int. Ed.* **2010**, *49*, 1258–1262.
- (4) Lässig, D.; Lincke, J.; Möllmer, J.; Reichenbach, C.; Möller, A.; Gläser, R.; Kalies, G.; Cychosz, K. A.; Thommes, M.; Staudt, R.; Krautscheid, H. *Angew. Chem.* **2011**, *123*, 10528–10532.
- (5) Lincke, J.; Lässig, D.; Moellmer, J.; Reichenbach, C.; Puls, A.; Moeller, A.; Gläser, R.; Kalies, G.; Staudt, R.; Krautscheid, H. *Microporous Mesoporous Mater.* **2011**, *142*, 62–69.
- (6) Reichenbach, C.; Kalies, G.; Lincke, J.; Lässig, D.; Krautscheid, H.; Moellmer, J.; Thommes, M. *Microporous Mesoporous Mater.* **2011**, *142*, 592–600.
- (7) Bauer, C. A.; Timofeeva, T. V.; Settersten, T. B.; Patterson, B. D.; Liu, V. H.; Simmons, B. A.; Allendorf, M. D. *J. Am. Chem. Soc.* **2007**, *129*, 7136–7144.
- (8) Harbuzaru, B. V.; Corma, A.; Rey, F.; Atienzar, P.; Jordá, J. L.; García, H.; Ananias, D.; Carlos, L. D.; Rocha, J. *Angew. Chem.* **2008**, *120*, 1096–1099.
- (9) Corma, A.; Garcia, H.; Llabres i Xamena, F. X. *Chem. Rev.* **2010**, *110*, 4606–4655.
- (10) Batten, S. R.; Neville, S. M.; Turner, D. R. *Coordination Polymers—Design, Analysis and Application*; RSC Publishing: Cambridge, U.K., 2009.
- (11) Robson, R. *J. Chem. Soc., Dalton Trans.* **2000**, 3735–3744.
- (12) Blatov, V. A.; Carlucci, L.; Ciani, G.; Proserpio, D. M. *CrystEngComm* **2004**, *6*, 377–395.
- (13) Baburin, I. A.; Blatov, V. A.; Carlucci, L.; Ciani, G.; Proserpio, D. M. *J. Solid State Chem.* **2005**, *178*, 2452–2474.
- (14) Alexandrov, E. V.; Blatov, V. A.; Kochetkov, A. V.; Proserpio, D. M. *CrystEngComm* **2011**, *13*, 3947–3958.
- (15) Baburin, I. A.; Blatov, V. A.; Carlucci, L.; Ciani, G.; Proserpio, D. M. *Cryst. Growth Des.* **2008**, *8* (2), 519–539.
- (16) Carlucci, L.; Ciani, G.; Proserpio, D. M. *Chem. Commun.* **2004**, 380–381.
- (17) Eddaoudi, M.; Kim, J.; Rosi, N.; Vodak, D.; Wachter, J.; O'Keeffe, M.; Yaghi, O. M. *Science* **2002**, *295*, 469–472.
- (18) Chui, S. S.-Y.; Lo, S. M.-F.; Charmant, J. P. H.; Orpen, A. G.; Williams, I. D. *Science* **1999**, *283*, 1148–1150.
- (19) Férey, G.; Mellot-Draznieks, C.; Serre, C.; Millange, F.; Dutour, J.; Surblé, S.; Margiolaki, I. *Science* **2005**, *309*, 2040–2042.
- (20) Horcajada, P.; Surblé, S.; Serre, C.; Hong, D.-Y.; Seo, Y.-K.; Chang, J.-S.; Grenèche, J.-M.; Margiolaki, I.; Férey, G. *Chem. Commun.* **2007**, 2820–2822.
- (21) Serre, C.; Mellot-Draznieks, C.; Surblé, S.; Audebrand, N.; Filinchuk, Y.; Férey, G. *Science* **2007**, *315*, 1828–1831.
- (22) Hunger, J.; Krautscheid, H.; Sieler, J. *Cryst. Growth Des.* **2009**, *9*, 4613–4625.
- (23) Lincke, J.; Lässig, D.; Stein, K.; Moellmer, J.; Kuttathayil, A. V.; Reichenbach, C.; Moeller, A.; Staudt, R.; Kalies, G.; Bertmer, M.; Krautscheid, H. *Dalton Trans.* **2012**, *41*, 817–824.
- (24) Lässig, D.; Lincke, J.; Krautscheid, H. *Tetrahedron Lett.* **2010**, *51*, 653–656.
- (25) Blatov, V. A. TOPOS Version 4.0. In *IUCr CompComm Newsletter*, Vol. 7; 2006; pp 4–8. (Available via the Internet at <http://www.topos.ssu.samara.ru>.)
- (26) Spek, A. L. *J. Appl. Crystallogr.* **2003**, *36*, 7–13.
- (27) Lässig, D.; Lincke, J.; Griebel, J.; Kirmse, R.; Krautscheid, H. *Inorg. Chem.* **2011**, *50*, 213–219.

(28) Zhang, J.-P.; Lin, Y.-Y.; Zhang, W.-X.; Chen, X.-M. *J. Am. Chem. Soc.* **2005**, *127*, 14162–14163.

(29) Sheldrick, G. M. *Acta Crystallogr., Sect. A: Found. Crystallogr.* **2008**, *A64*, 112–122.